Stopping power of a buffer gas for laser plasma debris mitigation

Davide Bleiner[1,a] and Thomas Lippert[2]
[1]*ETH Zurich, Sonneggstrasse 3, 8092 Zurich, Switzerland*
[2]*Paul Scherrer Institute, 5232 Villingen-PSI, Switzerland*

(Received 19 June 2009; accepted 10 November 2009; published online 18 December 2009)

The stopping power of a buffer gas against laser-plasma debris is quantitatively assessed by means of visualization techniques. For ablation of planar tin targets in an Ar ambient, an expanding wavefront was visualized, whose translation energy was rapidly reduced within a few millimeters above the target surface. The fastest debris component was along the normal to the target with an initial kinetic energy of 1.1 keV. The buffer gas efficiency changed in a line-of-sight-dependent way, thermalizing more efficiently the on-axis components. The maximum stopping power of the gas buffer was determined as high as 0.4 keV/mm. Due to the reduction in stopping power, nonlinearly with the debris kinetic energy, a gas buffer thickness of 10 mm is required at the studied atmospheric pressure in order to mitigate high energy debris below a fiducial threshold of 0.1 keV. © *2009 American Institute of Physics*. [doi:10.1063/1.3271142]

I. INTRODUCTION

Laser plasma debris mitigation with electromagnetic fields, rotating foil traps, or gas curtain has been investigated to try to mitigate the problem of fast laser-induced shrapnel interacting with the beam delivery or radiation collection optics, as for instance in extreme ultra-violet (EUV) sources.[1–3] Among these mitigation techniques, the buffer gas has shown the advantage to operate also on the neutral debris.[4] Soer *et al.*[5] investigated debris mitigation for EUV sources using directional gas flows. The purpose of the gas flow was to change the direction of the particles such that a trap can subsequently capture them. Two types of gas flows were considered: (i) longitudinal gas flows, i.e., with a flow direction essentially parallel to the velocity of the debris particles, and (ii) transversal gas flows, having a flow direction essentially perpendicular to that of the particles. The experiments showed that directional gas flows suppress debris in the same way a buffer gas does, unless the flow velocity becomes of the same order as the thermal velocity of the gas. Harilal *et al.*[6,7] studied ion debris mitigation from tin laser-produced plasmas (LPPs) using ambient gas, magnetic field, and combined effects. Tin ion penetration ranges into buffer gases were estimated using the Monte Carlo simulation code SRIM and compared with experimental results. The presence of a transverse magnetic field of 0.64 T slowed the propagation of fast moving tin ions but failed to stop them. The synergistic effect of a combination of magnetic field and an ambient gas was proposed to be promising for mitigating tin ions, although quantitative information on buffer gas stopping power was not given.

Therefore, experimental data of the behavior of the buffer gas are important to quantify the stopping power ability. The buffer gas's stopping power could not be determined so far by means of mass spectrometry, e.g., measuring the debris kinetic energy (KE) with a quadrupole mass filter or time-of-flight mass analyzer, because of (i) conflict among vacuum requirements for mass spectrometry and need to inject significant buffer gas mass flows. (ii) Neutrals are measured with electron impact sources, which become ineffective in the presence of a background gas. Moreover, the ability to acquire simultaneously the motion as a function of ejection angle from the spot site (line of sight) would be time consuming, when not too expensive, by means of angle-resolved spectroscopy. Here line of sight means angle with the target normal that is also the laser beam direction. Finally, another issue is important to explain the lack of cross-section data at typical laser plasma energies of 0.1–3 keV. In fact, at high energy (MeV), a "*hard sphere*" cross section is a good approximation. This depends on the actual ion and neutral radii. At low energy, as in the present case, ion-dipole interaction is important, and the bare radii of the projectile and the target are less informative. Considering Ar as buffer gas, Ar dipole moment is zero, but it is polarizable, and Langevin cross section is a good approximation in such case.

The approach to overcome these limitations is based on fluid dynamics imaging techniques, which enable two-dimensional visualization of the laser-induced debris expansion in a buffer gas, as a function of time. Imaging techniques are also compatible with any ambient pressures and any particle form, i.e., neutrals too. The imaging of a flow presumes to operate in a continuum fluidlike regime. The fluid is a coupled ensemble of particles, whose macroscale characteristics dominate over their atomistic nature. The relevant information for debris mitigation is the fluid KE and flow directionality. Debris mitigation indeed becomes less important for rarefied ensembles, i.e., when the LPP is far from the optics.

Henceforth, the aim of this work was to measure the KE loss per unit distance of a laser-induced plume (or stopping power of an ambient gas) as a function of line of sight. The plume was visualized at different times by means of a well-established technique in fluid mechanics, i.e., shadowgraphy.[8] The images captured at specific time delays permitted to evaluate the KE as a function of space and time.

[a]Electronic mail: bleinerd@ethz.ch.

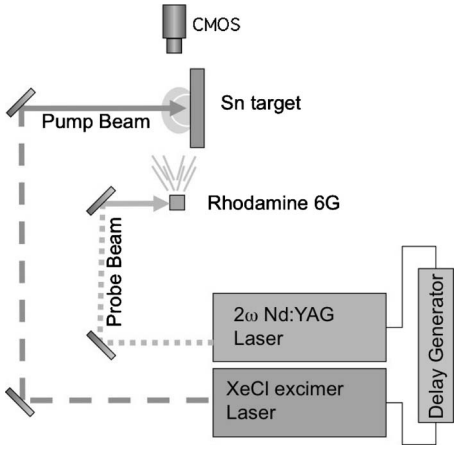

FIG. 1. Shadowgraphy setup for the pump-probe experiments.

II. METHODS

In the shadowgraphy setup (Fig. 1) the *pump* beam was a XeCl excimer laser (wavelength of 308 nm, pulse width of 25 ns full width at half maximum) with output energy of 75 mJ, and an attenuator was used along the beam path to adjust the energy delivered onto the sample. The laser intensity was approximately 10^{10} W/cm^2. The beam was focused with a plano-convex lens to obtain a spot of 150 μm at a distance slightly shorter than the focal length to prevent gas breakdown.

Back illumination was obtained by a probe laser (Nd:yttrium aluminum garnet, $\lambda=532$ nm, $t=6$ ns) pumping a fluorescent dye (rhodamine 6G), placed on the camera axis on the opposite target side. The delay between the pump and probe laser pulses was set by a digital pulse/delay generator with minimum delay of 5 ns. A complementary metal-oxide semiconductor (CMOS) camera allowed visualization of the process with a microscopic objective focused on the ablation region. The target was a high purity tin planar sample. Further details on the setup are given in previous publications.[9,10] Upon ablation, the released plume as well as the induced pressure wave caused a local difference of the ambient gas refractive index that could be monitored on the camera imaging. Regions of lower density were underilluminated by means of divergent refraction, and regions of higher density were brighter because of tighter probe field collimation. In this very setup, the target was mounted inside a gastight chamber so that a controlled argon atmosphere could be formed. The pressure here was atmospheric (10^5 Pa) and at room temperature (STP). The images were used to define the advancement distance as a function of time delay between laser pulse and acquisition. The advancement speed could be determined on a instantaneous basis, and all these points were postprocessed to define the deceleration profile.

III. RESULTS AND DISCUSSION

In a previous work,[11] it was shown that the background gas in an ablation environment has, or has not, the capability to confine and thermalize the ablated species depending on the scattering cross section. *Thermalization* is the process of fast particle interaction with the buffer gas toward a thermal equilibrium. The laser-induced ejection of Si atoms was shown to produce a wedgelike opening into the contact front,[12] i.e., a column of fast tiny shrapnel was imaged cutting through the advancing bow. On the other hand, laser-induced Sn particles remained trapped within the advancing high density front. The capability of a background gas to confine and thermalized tin-related debris[11] has motivated the use of background gases as buffers to protect the optics.

Figure 2(a) shows a shadowgraphy image at 500 ns delay, highlighting the outer bow shock and the trapped hemisphere. The larger bow shock is produced during surface irradiation, slightly prior to ablation. The radiation pressure can be calculated with the relation $p=(1+R)I/c$,[13] where I is

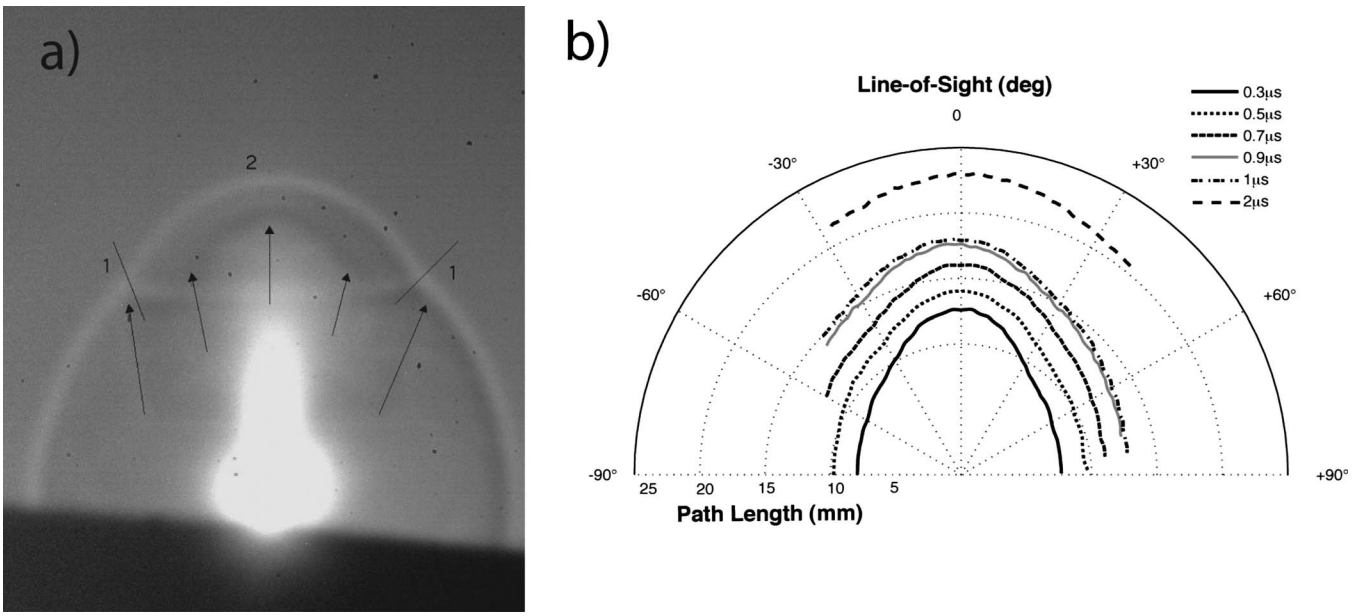

FIG. 2. Wave front progression in the background gas. (a) Shadowgraphy image at 500 ns delay highlighting the unperturbed bow shock edge (1) and the thrust bow front (2) trapping the debris. The field width is approximately 20 mm. (b) Front traces as a function of time.

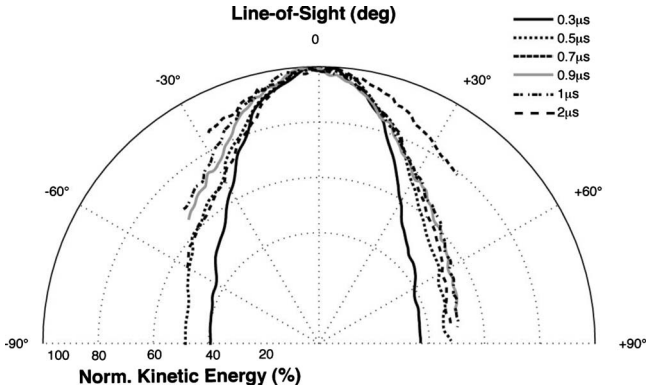

FIG. 3. Normalized KE profiles as a function of time for the wave fronts of Fig. 1.

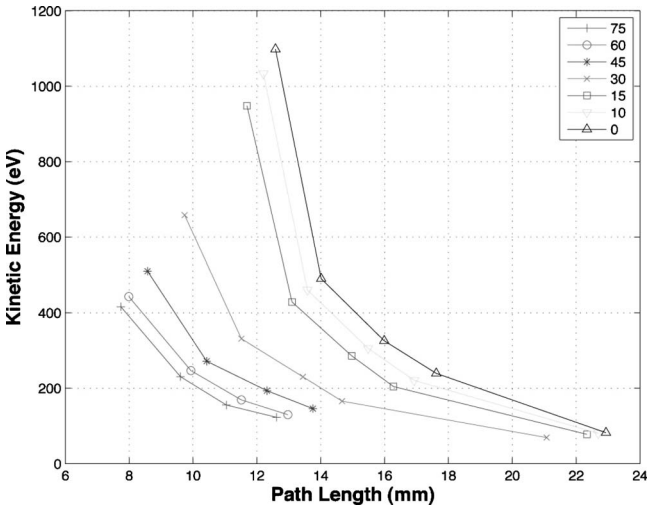

FIG. 4. KE vs distance for a selection of line of sights given as off-normal angle.

the laser intensity in W/cm^2, R is the surface reflectivity, and c is the speed of light. The tin surface reflectivity for the XeCl 308 nm photon (4.0 eV) is 75%.[14] The obtained radiation pressure onto the irradiated spot is 0.6 MPa. This pressure is exerted in the time scale of the laser pulse duration, i.e., 25 ns, which is a sudden change inducing a bow shock. The computed energy is 14.5 mJ, which is a conversion efficiency of 19.4% from the input value of 75 mJ. The energy losses are due to reflectivity. The bow shock expands hemispherically and is forward offset by the ablated debris in a snowplough effect. The width of the axial forward-pushed front [front "2" in Fig. 2(a)] stretches as wide as the emittance of the debris. Debris is henceforth lagged and confined within the axial region, as indicated by the arrows in Fig. 2(a).

Figure 2(b) shows the acquired contact fronts at different time slices. The laser beam irradiates the center of the polar grid from above and the front expands outward in the shown hemisphere. The polar coordinates permit to visualize the radial expansion across several lines of sight. The lines of sight can be intended as directions toward the EUV collector, which typically spans over 130°–150°. Although the angular span plotted is 180° (2π sr), the acquisition traces are limited by the field of view. Henceforth, the aged stages are clipped at the borders. The early stages are characterized with a predominant forward thrust in a region of ±15° off-normal, almost as a one-dimensional layer, which confirms previous observations.[15] After 500 ns, significant background gas deceleration of the forward front reduces the speed bias between the front and the lateral portions. Hence, the sharpness of the front is less and less pronounced as times goes by. Following the well-established $\cos^p \theta$ model,[16] the background gas induces a time-dependent reduction in the exponent p of approximately 50%.

Figure 3 shows the flattening of the debris advancement fronts as a function of time, presented as normalized KE (absolute values are discussed below). This plot permits to visualize the deceleration of the background gas, which is concentrated along the longitudinal direction of motion. The transverse direction is less affected by the background gas, as demonstrated by the fact that the profiles overlay as long as 1 μs. For a time of >1 μs the momentum is less heterogeneous as a function of line of sight due to a significant homogenization of the forward speed to the radial one. Hence a characteristic time scale for gas buffer operation is of the order of 1 μs.

Figure 4 shows the KE along a representative selection of line of sights. The KE was computed multiplying the half atomic mass *times* the square of the line-of-sight speed, obtained from the front position change within the known time delay difference. The mass is that of atomic tin. Bulky dusty particles are not considered here as the measurements highlighted their occurrence on a longer time scale of a few μs's. Besides, dusty particles are prone to veneer the optics surface and are therefore out of the scope of this erosion mitigation study. Considering that the profiles shown are symmetric, it is indicative to show line of sights in the positive angular quadrant. The peak KE is attained in the early stage (i.e., at short path length) in the axial front region (0° angle). The latter value was observed to be as high as 1.1 keV. The braking action of the gas buffer induces a distance-dependent KE loss, with a nominal suberosive magnitude ($<$0.15keV) attained over 5–10 mm, depending on the initial energy (see below).

The spatial distribution of the KE permits to determine the gas-related stopping power and scattering cross section. The stopping power dK/dx is the loss of KE (K) for a given space interval.[17] The stopping power of the gas curtain is influenced by the collision frequency—number of collision per unit time. Henceforth, the stopping power is a function of time because the steady reduction in speed influences the collision frequency which influences back the speed in a loopwise way.

The stopping power reduces progressively with the reduction in KE, which explains the variation for various line of sights and for larger path lengths. The stopping power versus the thermalized KE is shown in Fig. 5. Each stopping power point is referred to as specific $\Delta KE = K_{init} - K_{fin}$, with $K_{init} > K_{fin}$ because the thermalization has reduced the energy of the fast drift component and made it closer to that of the ambient buffer gas that is a thermal speed equilibrium. The

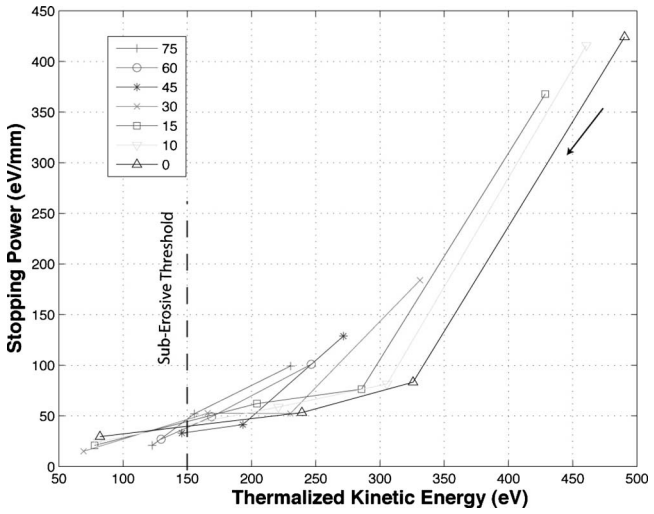

FIG. 5. Stopping power vs the thermalized KE for a selection of line of sights. A nominal threshold for debris erosion to the collector bilayers is given for reference as found from the data in Wu. The arrows indicate the temporal evolution of the debris energetics.

"thermalized KE" refers to the KE following collisions across the gas curtain thickness. Thus, in the diagram the KE value is the lower one K_{fin}, i.e., *after* the thermalization. One notes that the highest stopping power is obtained for the on-axis fast component in the early expansion stage. The maximum value for Ar background in combination with Sn debris is approximately 425 eV/mm, which thermalizes the keV component to 475 eV within slightly less than 2 mm. The stopping power is indeed progressive, i.e., stronger at higher KE, milder at lower KE.

The stopping power is related to the scattering cross section with the following relation: $\sigma=(dK/dx)/K\,n$, where besides the above introduced symbols, n is the buffer gas number density.[18] The obtained cross section is shown in Fig. 6 for three lines of sight. One notes that the cross section is drastically reduced at low KE (progressive action of gas buffer). The average cross section for the slower debris is around 1.3×10^5 b depending on the line of sight. For debris faster than 0.3 KeV the collision cross section is up to a factor of 3 larger.

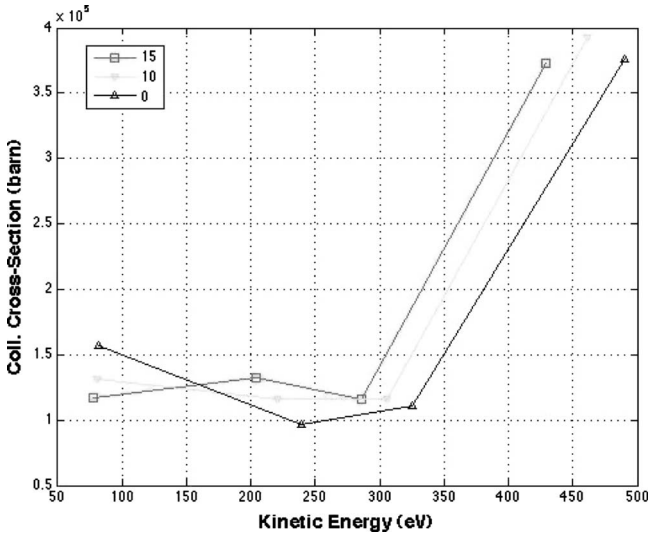

FIG. 6. Collision cross section as a function of KE and line of sight for the axial components of the ejected debris. The use of a gas buffer is a factor of 3 more effective to thermalize fast debris, namely, KE$>$0.3 keV.

In order to mitigate the erosive effects of the debris showering on to the mirror, one needs to moderate the KE below a specific erosive threshold value. The sputter yield of Ar is studied in Wu *et al.*[19] From that study we picked up a nominal value of 0.15 keV as the "erosive threshold." This value is nominal in the sense that erosion can occur also at lower KE. Nevertheless, the extent of it is of 0.3 eroded atoms per impinging bullet (sputter yield) at the chosen threshold. Moreover, the 1:3 yield rapidly drops at lower KE, such that at 50 eV the sputter yield is reported in Wu *et al.*[19] as 1:100.

The visualized fronts were advancing and decelerating against a stagnant background at standard room conditions (STP). Henceforth, from the experimental data acquired one concludes that at 10^5 Pa pressure a critical thickness of 10 mm of Ar is required to fully mitigate even the fast axial component. This critical thickness scales up at reduced pressure in order to maintain the same number of thermalizing collisions.

IV. CONCLUSIONS

Gas buffers to protect the collection optics from debris in a LPP source have the implicit advantage to buffer both charged and neutral particles. Thermalizing collisions are responsible for the mitigation of the KE down to a suberosion threshold. The stopping power was quantified to be as effective as 0.4 eV/mm. The stopping power is, however, a progressive function of KE, being therefore more effective along the axial (fast) component. *Full buffering* of laser-induced tin debris' tendency to erosion required an Ar gas buffer characteristic thickness of >10 mm (or characteristic thermalization times of 1 μs) at 10^5 Pa. Collision cross sections of 1.3×10^5 b were obtained at the steady state. The cross section profile versus KE showed that a gas buffer is a factor of 3 more effective to thermalize fast debris (Fig. 6).

[1] R. C. Spitzer, T. J. Orzechowski, D. W. Phillion, R. L. Kauffman, and C. Cerian, J. Appl. Phys. **79**, 2251 (1996).
[2] S. A. George, W. T. Silfvast, K. Takenoshita, R. T. Bernath, C. S. Koay, G. Shimkaveg, and M. C. Richardson, Opt. Lett. **32**, 997 (2007).
[3] N. Fornaciari, R. Kanouff, and P. Michael, "Discharge source with gas curtain for protecting optics from particles," Report No. PCT/US2002/024092, 2002.
[4] M. P. Kanouff and A. K. Ray-Chaudhuri, Proc. SPIE **3676**, 735 (2003).
[5] W. Soer, D. Klunder, M. van Herpen, L. Bakker, and V. Banine, Proc. SPIE **6151**, 1093 (2006).
[6] S. S. Harilal, B. O'Shay, Y. Tao, and M. S. Tillack, Appl. Phys. B: Lasers Opt. **86**(3), 547 (2007).
[7] S. S. Harilal, B. O'Shay, M. S. Tillac, and Y. Tao, J. Appl. Phys. **99**, 083303 (2006).
[8] G. S. Settles, *Schlieren & Shadowgraphy Techniques* (Springer, New York, 2006).
[9] R. Fardel, M. Nagel, F. Nüesch, T. Lippert, and A. Wokaun, Appl. Surf. Sci. **255**, 5430 (2009).
[10] M. Hauer, D. J. Funk, T. Lippert, and A. Wokaun, Opt. Lasers Eng. **43**, 545 (2005).
[11] D. Bleiner and A. Bogaerts, Spectrochim. Acta, Part B **61**, 421 (2006).
[12] G. Callies, P. Berger, and H. Hugel, J. Phys. D **28**, 794 (1995).
[13] D. Attwood, *Soft X-Rays and Extreme Ultraviolet Radiation: Principles and Applications* (Cambridge University Press, Cambridge, England, 2007).

[14]G. Jezequel, J. C. Lemonnier, and J. Thomas, J. Phys. F: Met. Phys. **7**, 2613 (1977).
[15]D. Bleiner, A. Bogaerts, F. Belloni, and V. Nassisi, J. Appl. Phys. **101**, 083301 (2007).
[16]K. Saenger, in *Pulsed Laser Deposition*, edited by D. B. Chrisey and G. K. Hubler (Wiley, New York, 1994).
[17]J. F. Ziegler, J. P. Biersack, and U. Littmark, *The Stopping and Range of Ions in Matter* (Pergamon, New York, 1985), Vol. 1.
[18]I. H. Hutchinson, Introduction to Plasma Physics, http://silas.psfc.mit.edu/introplasma, 2001.
[19]S. M. Wu, R. van de Kruijs, E. Zoethout, and F. Bijkerk, J. Appl. Phys. **106**(5), 054902 (2009).